Damping RF waves with low reflection in simulations of slab or curved magnetized plasma: parametrization, verification and implementation of Bermudez Perfectly Matched Layers

Laurent Colas[1,*], *Guillaume* Urbanczyk[2], *Walid* Helou[3], *Julien* Hillairet[1], and *Vincent* Maquet[4]

[1]CEA, IRFM, F-13108 Saint Paul Lez Durance, France.
[2]Institut Jean Lamour, UMR 7198 CNRS-Université de Lorraine, Campus Artem, 2 allée André Guinier, 54011 Nancy, France.
[3]ITER Organization, Route de Vinon-sur-Verdon, CS 90 046, 13067 St. Paul Lez Durance Cedex, France.
[4]Laboratory for Plasma Physics, LPP-ERM/KMS, 1000 Brussels, Belgium.

Abstract. Most Radio-Frequency antenna simulations in magnetic fusion require emulating radiation at infinity at some boundaries of the simulation domain. To this end, the Perfectly Matched Layer (PML) technique amounts to stretching artificially the (real) spatial coordinates into the complex plane. Following reference [1], this contribution parametrizes, tests numerically and implements unbounded stretching functions, whose only numerical limitations arise from the PML discretization: refining the mesh can reduce the spurious reflections from the PML arbitrarily low, at the expense of a larger numerical cost. We tune the PML to ensure low wave reflection in a prescribed spectral range [$k_{n,min}$, $k_{n,max}$] in a direction **n**, with a minimal discretization (*i.e.* at a minimal computational cost). We extensively quantify the reflection coefficients using 1D Finite Element simulations. The minimal discretization for a regular mesh scales as $k_{n,max}/k_{n,min}$. We extend the PML formulation to a cylindrical geometry, where the wave eigenmodes involve Bessel functions. We implement slab radial and parallel Bermudez PMLs in realistic multi-2D RF simulations [2], to attenuate the propagative Slow Waves parasitically emitted by the ITER ICRF antenna into a tenuous scrape-off layer.

1 Introduction

Most numerical simulations of Radio-Frequency (RF) antennas radiating into magnetic fusion plasmas are computationally demanding. Limited computer resources allow only modelling the immediate vicinity of the radiating elements with a sufficient spatial resolution. Emulating radiation at infinity is then necessary at some boundaries of the simulation domain. To damp the outgoing waves in boundary zones patched to the main simulation domain, the Perfectly Matched Layer (PML) technique amounts to locally stretch artificially the (real) spatial coordinates into the complex plane [3]. While the RF simulations in magnetic fusion abundantly use polynomial stretching functions (*e.g.* [4-9]), their finite coordinate stretching induces residual wave reflection from the PML that intrinsically limits the precision of the results, even in the continuous limit (infinitely fine discretization). One can however quantify and therefore control this residual reflection within a relevant spectral range, by adjusting the PML parameters [4] [10]. But the associated PML discretization may become numerically costly. Following reference [1], this contribution parametrizes, tests numerically and implements a class of unbounded stretching functions, whose only numerical limitations arise from the PML discretization: refining it can reduce the reflections arbitrarily low, at the expense of larger CPU/RAM requirements. In Cartesian and cylindrical coordinates, we show how to tune the PML parameters so that, once discretized, it is efficient inside some prescribed spectral range, at a minimal numerical cost. Earlier literature claims that this cost can be particularly low [1] [11]. We re-assess this cost as a function of the spectral range and of the PML location. We illustrate the technique with demanding multi 2-dimensional (2D) simulations of propagative Slow Waves in the Ion Cyclotron Range of Frequencies (ICRF) for ITER, whose results are detailed in reference [2].

Although the techniques below apply to a large variety of wave equations across many disciplines, we will discuss more specifically time-harmonic electromagnetic waves oscillating as $\exp(+\mathrm{i}\omega_0 t)$ with pulsation ω_0, governed by the Helmholtz equation for the complex electric field **E**.

$$\nabla \times (\boldsymbol{\mu}_\mathbf{r}^{-1} \nabla \times \mathbf{E}) - k_0^2 \mathbf{K}\mathbf{E} = \mathbf{0}\,. \qquad (1)$$

Here $k_0=\omega_0/c$ is a wavevector in vacuum, c is the velocity of light in vacuum, $\boldsymbol{\mu}_\mathbf{r}=\mathbf{1}$ is a (normalized) magnetic permeability tensor and **K** is a (normalized) dielectric tensor of the form [12]

$$\mathbf{K} = \begin{bmatrix} K_\perp & +\mathrm{i}K_\times & 0 \\ -\mathrm{i}K_\times & K_\perp & 0 \\ 0 & 0 & K_\parallel \end{bmatrix}. \qquad (2)$$

* Corresponding author: laurent.colas@cea.fr

This gyrotropic expression describes a homogeneous cold magnetized plasma whose background magnetic field $\mathbf{B_0}$ is oriented along the z direction.

2 Bermudez PMLs in Cartesian coordinates

The eigenmodes of equation (1) with separable Cartesian coordinates are plane waves oscillating spatially as exp(-i**k.r**). The allowed **k** values solve a specific dispersion relation, whose precise form depends on the plasma parameters, on the RF frequency range (ion cyclotron, helicon, lower hybrid…) and on the wave polarization [12]. Radiation at infinity means that all the wave-packets whose group velocity $\partial\omega_0/\partial\mathbf{k}$ points towards the exterior regions should leave the main simulation domain without being reflected. In addition, no wave-packet with inward group velocity should penetrate. Cartesian PMLs are buffer regions patched to the main simulation domain (see *e.g.* Figure 4a below). They aim at attenuating the relevant outgoing plane waves along the specific direction **n** normal to the plasma / PML boundary. Near the corners of the simulation domain, one may simultaneously specify several directions for the damping [4]. Assuming $|\mathbf{n}|=1$, the relevant quantities for formulating a PML are the normal components $r_n \equiv \mathbf{r.n}$ and $k_n \equiv \mathbf{k.n}$ [13]. If **n** points outwards, outgoing forward (resp. backward) waves in direction **n** feature $k_n>0$ (resp. $k_n<0$), *i.e.* their phase and group velocities, projected along **n**, are parallel (anti-parallel) [13].

2.1 PML formulation as coordinate stretching

One possible PML formulation consists in modifying the original problem (1) locally in the PML region so that, in the expression of the relevant outgoing plane waves, the (real) spatial coordinate r_n is replaced with an artificially stretched coordinate $t_n(r_n)$ such that

$$dt_n = S_n(r_n)\, dr_n \ , \qquad (3)$$

where $S_n(r_n)$ depends exclusively on r_n and not on other coordinates. One can implement the stretching *via* local artificial modifications of the plasma properties $\mathbf{K}(S_n, t_n)$. and $\boldsymbol{\mu}_\mathbf{r}(S_n, t_n)$ in the PML domain, as detailed in [3] [10] for several coordinate systems. References [4], [6] and [10] tested numerically this technique, in 2D or 3D with gyrotropic tensors described by (2). In the main simulation domain, the stretching function $S_n(r_n)=1$ and the original problem (1) remains unchanged. In the PML domain, and in the continuous limit, the modified (artificial) eigenmodes now vary spatially as exp[-i$k_n.t_n(r_n)$]: they can be damped if $\mathrm{Im}[k_n t_n(r_n)] < 0$. Attenuation of forward (backward) waves along **n** occurs if S_n incorporates an imaginary part with negative (positive) sign. It is then obvious that the stretching function cannot be adapted to both types of modes simultaneously. In magnetized plasmas, one can generally avoid the coexistence of forward and backward waves by choosing **n** either parallel or normal to $\mathbf{B_0}$ [6] [13]. Without loss of generality, we treat below the case of forward waves.

2.2 Parametrization of Bermudez PML

Once we comply with the above requirements, some latitude still remains to define the coordinate stretching functions $S_n(r_n)$. We suppose that the PML region spans the domain $r_n \in [r_{n0}, r_{n1}]$ while the main simulation domain locates in $r_n<r_{n0}$. For most stretching functions in the literature, $\mathrm{Im}[t_n(r_{n1})]$ remains finite. Consequently, residual wave reflection can occur at the PML extremity, even in the continuous limit, depending on the boundary conditions there. One can specify the PML so that $|\mathrm{Im}[k_n t_n(r_{n1})]|$ is large enough for all relevant k_n values. However, too large $|\mathrm{Im}[k_n t_n(r_n)]|$ may increase the numerical cost of the discretization. We explore here a class of unbounded stretching functions near $r_n=r_{n1}$. The PML reflectivity is null in the continuous limit: spurious reflection arises exclusively from the PML discretization and can be made arbitrarily small by refining the mesh, at the expense of a larger numerical cost. The stretching functions proposed by Bermudez [1] [11] write

$$S_n(r_n) = \begin{cases} 1, r_n < r_{n0} \\ 1 - \mathrm{i}\frac{\delta_0}{r_{n1}-r_n}, r_{n0} < r_n < r_{n1} \end{cases} . \qquad (4)$$

Length δ_0 defines the strength of the stretching and should be positive for forward waves. The stretched coordinate is

$$t_n(r_n) = \begin{cases} r_n, r_n < r_{n0} \\ r_n - \mathrm{i}\delta_0 \ln\left(\frac{r_{n1}-r_n}{\Delta r}\right), r_{n0} < r_n < r_{n1} \end{cases} , \qquad (5)$$

where $\Delta r \equiv r_{n1}-r_{n0}$ is the PML depth.

Δr, δ_0 and the number N_{PML} of element layers in the PML depth affect the PML properties and need to be adjusted properly. Only a regular meshing (element size $\Delta r/N_{PML}$) is studied below, although less structured meshes may be more efficient. N_{PML} influences the numerical cost of the PML and should be minimized. To develop PML tuning guidelines, we investigate the expected (artificial) RF field structure in the PML in the continuous limit, for an incoming plane wave with given k_n. Its shape is [11]

$$\mathbf{E}(r_n) \propto \left(\frac{r_{n1}-r_n}{\Delta r}\right)^{k_n\delta_0} \exp(-\mathrm{i}k_n r_n) \ . \qquad (6)$$

For the PML to behave properly, we infer that its discretization should resolve the spatial variations of the amplitude and the phase in (6). For the phase term this rule of thumb yields $N_{PML} > k_n\Delta r/2\pi$ [11]. Figure 1 plots the amplitude over the PML domain. When $k_n\delta_0 > 1$, the critical scale-length for the amplitude is the gradient length $\Delta r/(k_n\delta_0)$ at $r_n = r_{n0}$, imposing $N_{PML} > k_n\delta_0$. When $k_n\delta_0 < 1$, null amplitude decay lengths emerge from (6) in $r_n = r_{n0}+\Delta r$: one expects the PML reflectivity to rapidly degrade with decreasing $k_n\delta_0$. If $k_n\delta_0 = 1$ and $k_n\Delta r << 1$, the phase term hardly evolves over the PML domain, while the amplitude decays linearly. This decay exactly

matches the shape of a triangular finite element (FE), so that only one FE is necessary to produce the correct solution. Reference [11] identified this setting as optimal.

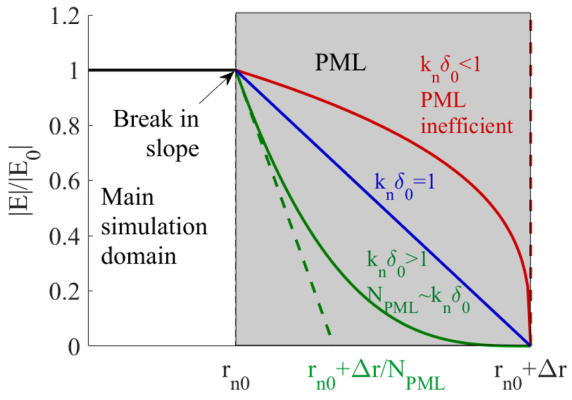

Fig. 1. Spatial variation of the amplitude of the artificial electric field (6) in the PML domain, for $k_n\delta_0$ lower or larger than unity, showing the typical scale-lengths to be resolved.

2.3 Numerical assessment in one dimension (1D)

To assess the above PML tuning guidelines, we conducted numerical tests in 1D using the Finite Element (FE) solver COMSOL. The model solves the 1D scalar wave equation

$$\partial^2_{\varphi\varphi}E(\varphi) + E(\varphi) = 0 \quad , \qquad (7)$$

where $\varphi \equiv k_n r_n$. Equation (7) does not retain all the complexity of the original equation (1) (*e.g.* tensorial dielectric properties, vector fields…). But, in the ICRF frequency range, if one isolates either the Fast or the Slow mode in 1 dimension, equation (1) reduces to an equation of type (7) for $\mathbf{n} \perp \mathbf{B_0}$. In view of section 4, a similar reduction also applies to the parallel PML for the Slow mode. The main simulation domain is the segment $[0, \varphi_0]$, with $\varphi_0 = k_n r_{n0} = 2\pi$, so that it represents one wavelength of the expected plane waves. The PML region is the segment $[k_n r_{n0}, k_n r_{n1}]$. Reference [11] extensively studied the phase term when $k_n\delta_0=1$. Therefore, we choose $k_n\Delta r_n=0.01$. We impose $E=E_0=1$V/m at $r_n=0$ and $E=0$ at $r=r_1$. As $S_n(r_n)$ in (4) is discontinuous across the plasma / PML interface (all the more as $\delta_0/\Delta r$ is large), so is $\partial_\varphi E$ in Figure 1. The FEs should have sufficiently large order to support this discontinuity. The FEs should also not cross the plasma/PML interface. We discretized the main simulation domain using quadratic Lagrange FEs with size 0.01 in normalized units. In the PML we scanned the number of FEs between 1 and 1024.

In the main simulation domain, the general solution of (7) compatible with the boundary condition in $r_n=0$ is

$$E(\varphi) = E_0 \frac{\exp(-i\varphi) + R\exp(+i\varphi)}{1+R} \quad . \qquad (8)$$

In this expression, the second term on the numerator is a wave reflected from the PML and R is a complex reflection coefficient. We assess the quality of the PML by estimating $|R|$ from the simulation results. For example

$$\frac{R}{1+R} = \left\langle \frac{E(\varphi)}{E_0} \exp(-i\varphi) \right\rangle \quad , \qquad (9)$$

where $\langle \cdots \rangle \equiv \frac{1}{2\pi}\int_0^{2\pi} \cdots d\varphi$ means spatial average over the main simulation domain (one wavelength). The data processing in (9) shifts the reflected wave to zero wavenumber and the incident wave to double wavenumber, so that the spatial averaging picks out only the reflected mode. Several alternative estimates for $|R|$ were also tested and exhibit qualitatively similar behaviour. Figures 2 plot $|R|$ from the above estimator versus $k_n\delta_0$, over the scan of N_{PML}.

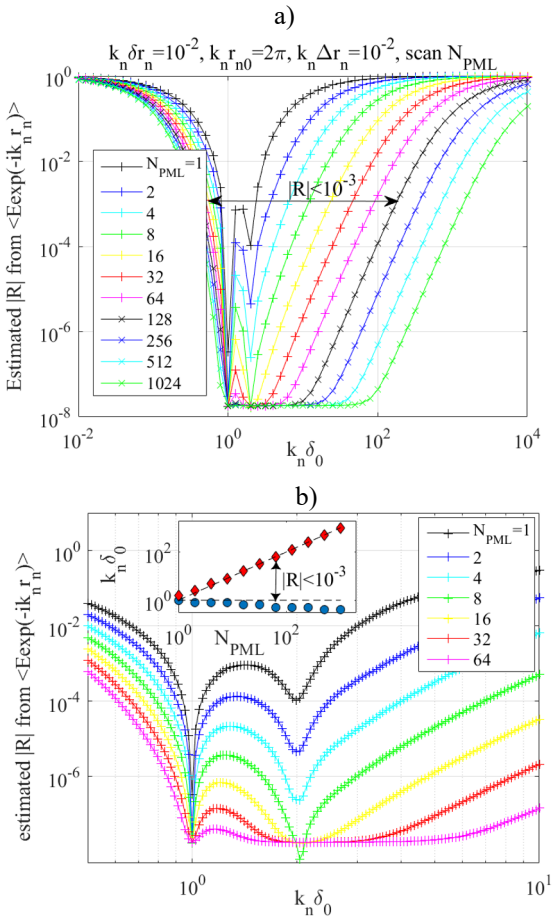

Fig. 2. a) $|R|$ estimated from (9) versus $k_n\delta_0$ in log-log scale over a scan of N_{PML}. Each point is a 1D simulation result. b) zoom over region [0.5, 10] in $k_n\delta_0$, with finer resolution of the curves. Inset: window in $k_n\delta_0$ for which $|R|<10^{-3}$, versus N_{PML}.

For $k_n\delta_0=1$ and $k_n\Delta r_n=0.01$, the PML behaves well, even for the minimal N_{PML}, consistent with [11]. However, for low values of N_{PML}, the peak in $|R|$ there is very sharp: when δ_0 is fixed, the PML reflection is low for nearly one single value of k_n. At fixed $k_n\delta_0$, $|R|$ decreases upon PML mesh refinement. A residual $|R|\sim 1.8\times10^{-8}$ remains. It depends neither on $k_n\delta_0$ nor on N_{PML} and may be due to the discretization of the main simulation domain, as observed in [11]. The range in $k_n\delta_0$ with low $|R|$ broadens with larger N_{PML}: its lower bound is close to 1 and it decreases slowly with increasing N_{PML}. Its upper bound is roughly

proportional to N_{PML}, consistent with the qualitative predictions. The exact upper bound value depends mainly on the requested $|R|$. In our tests, it is ~N_{PML} for $|R| \sim 10^{-3}$, showing good PML behaviour for $k_n\delta_0 \in [1, N_{PML}]$.

2.4 Optimizing the PML parameters for realistic wave spectra

Based on the above assessment, we would like now to ensure low PML reflection inside a prescribed spectral range, at a minimal numerical cost N_{PML}. Earlier literature [1] [11] mainly studied one single k_n value. In these conditions, Figures 2 show that an optimal choice is $k_n\Delta r \ll 1$ and $k_n\delta_0=1$. For this tuning, reference [11] showed a low reflectivity of the PML, independent of the PML parameters, even with a discretization as small as $N_{PML}=1$. Reference [11] presented the Bermudez stretching function as an "optimal" numerical choice, without free parameters. This approach is however not well adapted to realistic numerical simulations in magnetized plasmas, often featuring a broader spectrum $[k_{n,min}, k_{n,max}]$ at the plasma / PML interface (see *e.g.* section 4 and Figure 5 below). To optimize the PML, this spectrum should match the good $k_n\delta_0$ domain $[1, CN_{PML}]$ from Figures 2, where C is a numerical constant of order 1, depending on the requested maximal $|R|$. One should therefore take $\delta_0 \sim 1/k_{n,min}$. The minimal number of element layers across the PML depth is then $N_{PML} > k_{n,max}/Ck_{n,min}$. An optimal choice for the PML depth is $\Delta r \ll 1/k_{n,min}$. The maximal element size is finally $\Delta r k_{n,min}/k_{n,max} < C/k_{n,max}$.

3 Extension to cylindrical geometry

Most magnetic fusion devices feature curved geometry. Reference [10] tested numerically PMLs adapted to such curvature, in gyrotropic media. Reference [8] implemented such PMLs in realistic simulations. We would like here to extend the above analysis to a cylindrical geometry: we wish to stretch the usual cylindrical coordinates (r, θ, z) into the complex plane in order to emulate radiation conditions along the principal directions ($\mathbf{e}_r$, $\mathbf{e}_\theta$, $\mathbf{e}_z$). One can study the PML behaviour using the eigenmodes of RF wave equation (1) with separation of the cylindrical variables [3]. Assuming that $\mathbf{B_0}$ is along $\mathbf{e}_z$, these take the form [10] [14]

$$E(\mathbf{r}) \propto \begin{cases} H_m^{(1)}(k_\perp r)\exp(-\mathrm{i}k_\parallel z - \mathrm{i}m\theta) \\ H_m^{(2)}(k_\perp r)\exp(-\mathrm{i}k_\parallel z - \mathrm{i}m\theta) \end{cases} \quad (10)$$

respectively for forward and backward waves in direction $\mathbf{e_r}$. In this expression, the azimuthal mode number m is an integer, $H_m^{(1)}(Z)$ and $H_m^{(2)}(Z)$ are Hankel functions [15] and a dispersion relation similar to the Cartesian one links the squared wavevectors $k_\perp^2$ and $k_{//}^2$ [12].

3.1 Parametrization of Bermudez radial PMLs

From (10) we deduce that the PMLs in the axial and azimuthal directions are quite similar to the Cartesian PMLs. Without loss of generality, this sub-section treats radial PMLs adapted for forward waves in direction $\mathbf{e_r}$. One can deduce the behaviour of backward waves using $H_m^{(2)}(Z) = \bar{H}_m^{(1)}(\bar{Z})$ [15]. Unlike with Cartesian coordinates, the properties of the radial eigenfunctions, and therefore of the associated PML, depend on m and on the radial location r_0 of the plasma / PML interface, *via* the curvature of the circles r=constant. By analogy with the Cartesian case one can define a "local" radial wavevector

$$k_r^2(r_0, m) = k_\perp^2 - m^2/r_0^2 \ . \quad (11)$$

$k_r^2(r_0, m) > 0$ indicates that the eigenmode locally behaves as a propagating plane wave in the radial direction. This relation defines a maximal azimuthal mode number $m_{max} \equiv k_\perp r_0$ requiring attenuation in the PML.

To specify the PML parameters, we perform a qualitatively similar optimization as in the Cartesian case. Given $k_\perp$, m, r_0, Δr and δ_0, we first estimate the smallest scale-lengths for the (artificial) eigenmode (10) in the PML, in the continuous limit, once the radial coordinate r is stretched using formula (4). We deduce a minimal discretization necessary to resolve this specific mode. This estimate reads

$$N_{cyl} \approx k_\perp \Delta r \max_{r_0 \le r \le r_1} \left| \frac{H_m'^{(1)}[k_\perp t_r(r)]}{H_m^{(1)}[k_\perp r_0]} \right| |S_r(r)| \ , \quad (12)$$

where $H_m'^{(1)}$ denotes the derivative of the Hankel function with respect to its argument. From (12) one can deduce that small $k_\perp\Delta r$ is beneficial, similar to the Cartesian case. The asymptotic form of the Hankel function $H_m^{(1)}(Z)$ for large $|Z|$ (valid for r sufficiently close to r_1) is [15]

$$\left|H_m'^{(1)}(Z)\right| \approx \sqrt{\frac{2}{\pi|Z|}} \exp[\mathrm{Im}(Z)] \ , |Z| \gg 1 \ . \quad (13)$$

Formulas (13) and (5) tell that positive (negative) δ_0 is suitable for attenuating forward (backward) waves respectively. For $\delta_0>0$, formulas (5), (16) and (17) then yield close to $r=r_1$

$$\frac{\Delta r}{r_1 - r} \exp\left[k_\perp \mathrm{Im}\left(t_r(r)\right)\right] = \left(\frac{r_1 - r}{\Delta r}\right)^{k_\perp\delta_0 - 1} \ . \quad (14)$$

Formula (14) shows that N_{cyl} gets infinite when $k_\perp\delta_0 < 1$, qualitatively similar to the Cartesian case. If $k_\perp r_0 \gg 1$, formula (14) is valid all over the PML domain. When $k_\perp\delta_0 > 1$, (14) suggests that one should estimate N_{cyl} using $r=r_0$ in formula (12). One then gets a correction to the Cartesian formula within the WKB approximation

$$N_{cyl} \approx \left|\frac{H_m'^{(1)}(k_\perp r_0)}{H_m^{(1)}(k_\perp r_0)}\right| k_\perp |\Delta r - \mathrm{i}\delta_0|, k_\perp\delta_0 > 1 \ ,$$
$$\left|\frac{H_m'^{(1)}(k_\perp r_0)}{H_m^{(1)}(k_\perp r_0)}\right| \approx 1 - \frac{2m^2 - 1}{4(k_\perp r_0)^2} \ , k_\perp r_0 \gg m \ , \quad (15)$$

where $|m| < m_{max}$ means $|m|/(k_\perp r_0) < 1$. Asymptotic approximations of $H_m^{(1)}(Z)$ are also available for small values of the argument [15] and are given for m=0.

$$\left|\frac{H_0'^{(1)}(k_\perp r_0)}{H_0^{(1)}(k_\perp r_0)}\right| \approx -\frac{1}{k_\perp r_0[\ln(k_\perp r_0)+\gamma]}, k_\perp r_0 \ll 1 \ . \quad (16)$$

Figure 3 shows how the estimated N_{cyl} evolves with $k_\perp r_0$ and m at fixed $k_\perp \Delta r$ and $k_\perp \delta_0$>1. In this diagram, the Cartesian limit corresponds to $k_\perp r_0 \to \infty$ and is the same for all m values. When $|m|<k_\perp r_0$ larger N_{cyl} is associated with lower m, consistent with larger k_r from (11). For m=0, N_{cyl} is always larger than the Cartesian limit, and gets significantly larger as $k_\perp r_0$<1.

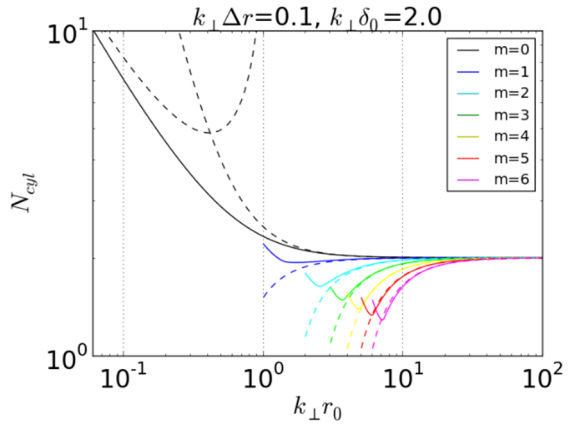

Fig. 3. N_{cyl} versus $k_\perp r_0$ in log-log scale over a scan of m, for $k_\perp \Delta r$=0.1 and $k_\perp \delta_0$=2. Only $k_\perp r_0 > m$ is drawn. Solid lines: general estimate (12). Dashed lines: simplified asymptotic formulae (15) and (16) for large and small $k_\perp r_0$.

3.2 Optimizing the radial PML parameters for realistic wave spectra

In realistic numerical simulations, the geometry of the problem generally imposes the radial location r_0 of the plasma / PML interface, as well as a relevant range of $k_\perp$ and m. We would then like to tune parameters Δr and δ_0 to ensure low PML reflection over this prescribed spectrum, at a minimal discretization N_{PML}. For one cylindrical mode, sub-section 3.1 showed that
1°) Δr should be as small as possible
2°) $k_\perp \delta_0$ should exceed 1
3°) if 2°) is fulfilled and all other parameters are fixed, N_{cyl} increases with δ_0
An optimal setting is therefore $\Delta r << 1/k_{\perp min}$ and $\delta_0 = 1/k_{\perp min}$, qualitatively similar to the Cartesian case. Once that r_0, Δr and δ_0 are set, one determines the minimal discretization of the PML depth from (12) as

$$N_{PML} = \max_{k_\perp,\ m \text{ range}} N_{cyl}(\Delta r, \delta_0, r_0, k_\perp, m)/C \ . \quad (17)$$

If $k_{\perp max} r_0 >> 1$, the Cartesian results apply for $k_\perp = k_{\perp max}$ so that $N_{PML} > k_{\perp max}/C k_{\perp min}$ in the cylindrical case.

4 Application to multi-2D slab slow wave simulations near the ITER ICRF antenna

The re-baseline of ITER in 2023 motivated a revision of sheath rectification estimates on its ICRF antenna port equipped with tungsten plasma-facing components [2]. Multi-2D RF-sheath estimates relied on the SSWICH-SW code [16], combining Slow Wave (SW) propagation from the antenna mouth to the Scrape-Off Layer (SOL), the excitation of RF oscillations in the sheath voltages at the antenna port sides and a subsequent Direct Current (DC) biasing of the SOL, using the multi-physics FE solver COMSOL. Figure 4a) sketches the 2-dimensional (2D: radial / parallel) RF simulation domain. It includes a private SOL representing the antenna port, followed by a free SOL where the SW can propagate. RF sheaths are treated as RF boundary conditions applied at both sides of the antenna port (blue boundaries) where we assess the Plasma Wall Interaction. To excite the Slow mode, we imposed at the antenna mouth (magenta boundary) maps of the near parallel RF electric field $E_{//}$ from the 3D antenna code TOPICA [17].

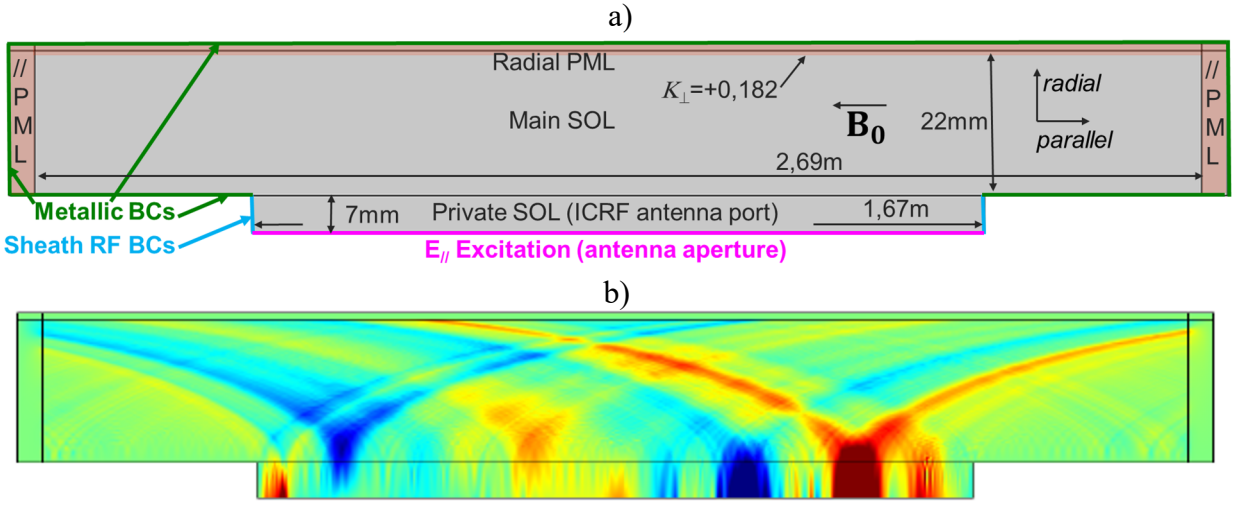

Fig. 4. a) 2D (radial / parallel) geometry (not to scale) of one SSWICH-SW run for scenario ITER low 2010. The reference dimensions of the simulation domain are indicated, as well as the boundary conditions (BCs) enforced at the different boundaries. b) Color map of simulated Im($E_{//}$) at altitude Y=0.1225m. The color scale is saturated to visualize the resonance cones in the main SOL.

Our simulation dataset included "low density" scenarios where $K_{//} < 0$ and $K_{\perp} > 0$ in (2) near the antenna. The cold SW then propagates along resonant cones (RC) emerging from the antenna mouth, up to the Lower Hybrid (LH) resonant layer, corresponding to $K_{\perp} = 0$, where they are absorbed [12]. Figure 4b illustrates a typical simulated $E_{//}$ field map for the Low 2010 ITER scenario [2], featuring very small scale-lengths. The particular SW dispersion relation allows all the small-wavelength modes to propagate far from the antenna. To resolve all scale-lengths, the full 2D mesh consists of 298787 domain elements and 3094 boundary elements (quadratic Lagrange FE). The simulated RF field patterns also exhibit strong anisotropy: the expected aspect ratio from the SW dispersion relation is $|K_{//}/K_{\perp}|^{1/2}$, reaching 86 at the inner part of the simulation domain, close to the LH resonance. We used elongated FEs with parallel resolution 7,5mm and radial one 0,1mm.

The transverse wavelength for the cold collision-less SW gets null as they reach the cold LH resonance, so that the simulation becomes intractable numerically. To emulate the presence of the LH resonance, we stopped the main simulation domain where $K_{\perp} = +0.182$, *i.e.* 2mm before the resonance radial position. We damped artificially the outgoing SW at the inner and lateral parts of the domain using slab Bermudez PMLs, implemented *via* artificial modifications of $K_{//}$ and $K_{\perp}$. We tuned the parallel PMLs to damp the typical emitted Slow Wave $k_{//}$ spectrum, obtained as the parallel Fourier transform of the excitation $E_{//}$ field map at the antenna mouth. The RC dispersion relation makes this spectrum relevant for the PMLs. Figure 5 shows a broad spectrum extending from $5m^{-1}$ to $35m^{-1}$, rather stable with the altitude.

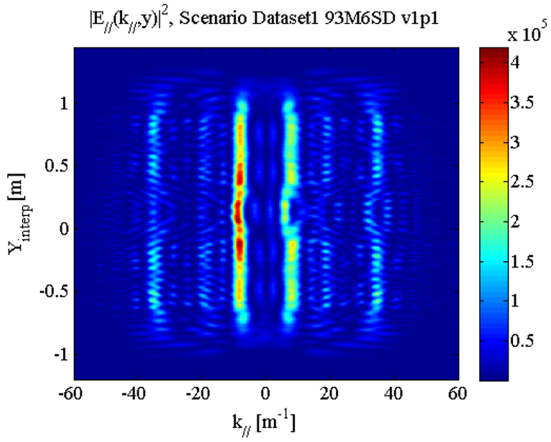

Fig. 5. Parallel Fourier transform of the complex $E_{//}$ RF field map from TOPICA applied at the ITER antenna mouth, versus $k_{//}$ and altitude of the 2D reference plane, for plasma scenario ITER low 2010. Antenna excitation: phasing [0, π, 0, π] and balanced power between the 4 toroidal rows of radiating straps

As the SW is forward in the parallel direction [6] [13], the spectral part with positive (negative) $k_{//}$ applies to the right-hand (left-hand) side parallel PML. In case of asymmetric antenna excitation, these two PMLs may be tuned differently. The radial PML drastically differs from the parallel ones. Firstly, the local $k_{//}$ and $k_{\perp}$ spectra differ by the aspect ratio $|K_{//}/K_{\perp}|^{1/2}$~86. In addition, the SW is backward in the radial direction [6], so that a negative δ_0 is required. For the reported simulation, the PMLs represented 5.75% of the mesh.

Figure 6 is a zoom on the upper-right part of Figure 4b. No reflected resonance cone is visible from the plasma / PML interfaces, demonstrating a good behaviour of the thin PMLs, despite a modest numerical cost. The parallel PML is insensitive to strong radial variations of the dielectric tensor: these variations do not affect the $k_{//}$ spectrum at the plasma / PML interface, and the radial discretization of the simulation domain was fine enough.

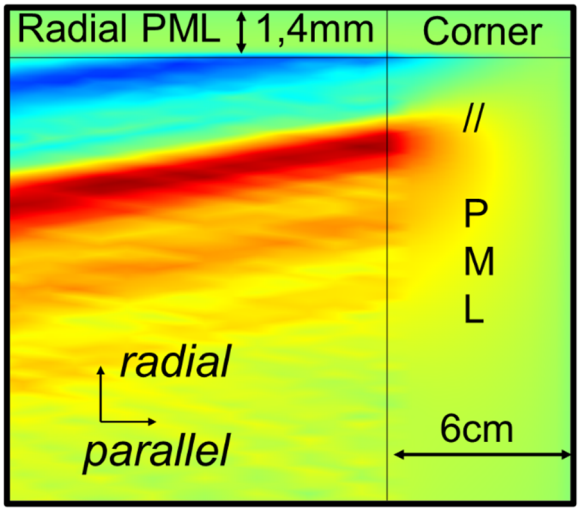

Fig. 6. Zoom on upper right part of Figure 4b, same color scale.

5 Discussion and outlook

This paper reported the first implementation of Bermudez PMLs for simulating RF waves in magnetized plasmas. These PMLs emulate unbounded coordinate stretching, *i.e.* feature no wave reflection in the continuous limit. In Cartesian and cylindrical coordinates, we showed how to optimize the PML parameters to ensure low wave reflection in a prescribed spectral domain at the plasma / PML interface, with a minimal discretization. This fine control capability is particularly attractive. The discretization can drop to N_{PML}=1 for narrow-band spectra [1] [11]. However, as all the PMLs relying on coordinate stretching [4] [10], the Bermudez one, once discretized, cannot be efficient over infinite spectral ranges: in Cartesian coordinates, we checked numerically that the minimal discretization N_{PML} scales as $k_{n,max}$ / $k_{n,min}$ for a regular PML mesh. Alternative meshings still need to be tested. The "optimality statement" in [11] may therefore need revision in the presence of broad spectra or in non-Cartesian coordinates. Coordinate stretching cannot attenuate simultaneously forward and backward waves. For magnetic fusion applications, modelling strategies exist to avoid the coexistence of forward and backward waves along a given direction [6] [13]. Finally, the discontinuous stretching function across the plasma / PML interface induces a discontinuity in some simulated

* Corresponding author: laurent.colas@cea.fr

RF field components. One should therefore carefully discretize the simulation domain. Alternative continuous unbounded stretching functions remove the latter constraint, at the expense of a possibly finer discretization [1]. Slab Bermudez PMLs behaved well in our ITER application with propagative Slow Waves in the Ion Cyclotron Range of Frequencies (analogous to Lower Hybrid waves), where the dielectric tensor was highly anisotropic and inhomogeneous. They are envisaged in future RF simulations of the WEST Travelling Wave Array [18]. Bermudez PMLs still need to be tested in situations more delicate computationally, *e.g.* full-wave simulations crossing a cold plasma resonance.

ITER simulations have been conducted under contract IO/23/CT/4300002873. The views and opinions expressed herein do not necessarily reflect those of the ITER Organization.

References

1. A. Bermúdez, L. Hervella-Nieto, A. Prieto, R. Rodriguez, An optimal perfectly matched layer with unbounded absorbing function for time-harmonic acoustic scattering problems, Journal of Computational Physics **223**, 469 (2007). https://doi.org/10.1016/j.jcp.2006.09.018
2. L. Colas, W. Helou, G. Urbanczyk, V. Bobkov, F. Calarco, N. Fedorczak, D. Milanesio and J. Hillairet, Numerical assessment of ICRF-specific Plasma-Wall Interaction in the new ITER baseline using the SSWICH-SW code, Nuclear Materials and Energy **42**, 101831 (2025) https://doi.org/10.1016/j.nme.2024.101831
3. F. L. Teixeira & W. C. Chew, Analytical Derivation of a Conformal Perfectly Matched Absorber for Electromagnetic Waves, Microwave and optical technology letters **17**, 231 (1998). https://doi.org/10.1002/(SICI)1098-2760(199803)17:4%3C231::AID-MOP3%3E3.0.CO;2-J
4. J. Jacquot, L. Colas, F. Clairet, M. Goniche, S. Heuraux, J. Hillairet, G. Lombard and D. Milanesio, 2D and 3D modeling of wave propagation in cold magnetized plasma near the Tore Supra ICRH antenna relying on the perfecly matched layer technique, Plasma Phys. Control. Fusion **55**, 115004 (2013). https://doi.org/10.1088/0741-3335/55/11/115004
5. L. F. Lu , L. Colas, J. Jacquot, B. Després, S. Heuraux, E. Faudot, D. Van Eester, K. Crombé, A. Křivská, J.-M. Noterdaeme, W. Helou and J. Hillairet, Modelling of radio frequency sheath and fast wave coupling on the realistic ion cyclotron resonant antenna surroundings and the outer wall, Plasma Phys. Control. Fusion **60** (2018) 035003 https://doi.org/10.1088/1361-6587/aaa030
6. M. Usoltceva, R. Ochoukov, W. Tierens, A. Kostic, K. Crombé, S Heuraux and J-M Noterdaeme, Simulation of the ion cyclotron range of frequencies slow wave and the lower hybrid resonance in 3D in RAPLICASOL, Plasma Phys. Control. Fusion **61** (2019) 115011, https://doi.org/10.1088/1361-6587/ab476d
7. L. F. Lu, L. Colas, L. Cao, G. Urbanczyk, B. Lu, Y. Q. Shen and X. J. Zhang, Self-consistent modelling of radio frequency sheath in 3D with realistic ICRF antennas, Nucl. Fusion **64** (2024) 126013 https://doi.org/10.1088/1741-4326/ad7c65
8. W. Tierens, A. Kumar, C. Klepper, J. Lore, J. R. Myra, J. Hillairet, G. Urbanczyk, W. Helou, L. Colas, A. Grosjean, J. Gunn and the WEST Team, Radiofrequency sheath rectification on WEST: first application of the sheath-equivalent dielectric layer technique in tokamak geometry, Nucl. Fusion **64** (2024) 126039 https://doi.org/10.1088/1741-4326/ad80a9
9. G. Urbanczyk, S. Shiraiwa, N. Bertelli, W. Tierens, R. Bilato, V. Bobkov, R. Ochoukov, R. Dux, L. Colas, J. P. Gunn, J. Hillairet, N. Fedorczak, R. Diab, L. Tsowemoo, J. Moritz, S. Heuraux, ASDEX Upgrade and WEST Teams, ICRF near-field effects sensitivity to magnetic tilt-angle, 25th Topical Conference on Radio-Frequency Power in Plasmas, Schloss Hohenkammer, Germany, May 19-22 (2025)
10. L. Colas, J. Jacquot, J. Hillairet, W. Helou, W. Tierens, S. Heuraux, E. Faudot, L. Lu, G. Urbanczyk, Perfectly Matched Layers for time-harmonic transverse electric wave propagation in cylindrical and toroidal gyrotropic media, Journal of Computational Physics **389**, 94 (2019) https://doi.org/10.1016/j.jcp.2019.02.017
11. R. Cimpeanu, A. Martinsson, M. Heilb, A parameter-free perfectly matched layer formulation for the finite-element-based solution of the Helmholtz equation, Journal of Computational Physics **296,** 329 (2015). https://doi.org/10.1016/j.jcp.2015.05.006
12. Thomas H. Stix, Waves in plasmas, (Springer Science & Business Media, 1992).
13. E. Bécache, P. Joly, M. Kachanovska, Stable perfectly matched layers for a cold plasma in a strong background magnetic field, Journal of Computational Physics **341**, 76 (2017). https://doi.org/10.1016/j.jcp.2017.03.051
14. W.P. Allis, S.J. Buchsbaum, A. Bers, Waves in Anisotropic Plasmas, (MIT press, 1963)
15. M. Abramowitz & I. Stegun, Handbook of mathematical functions, (Dover, 1972).
16. J. Jacquot, D. Milanesio, L. Colas, Y. Corre, M. Goniche, J. Gunn, S, Heuraux, M. Kubič., Radio-frequency sheaths physics: Experimental characterization on Tore Supra and related self-consistent modelling, Physics of Plasmas **21**, 061509 (2014). https://doi.org/10.1063/1.4884778
17. D. Milanesio, W. Helou, V. Polli, F. Durodié, P. Lamalle, V. Maquet, A. Messiaen, W. Tierens and W. Zhang, Recent modeling for the ITER ion cyclotron range of frequency antennas with the

TOPICA code, Nucl. Fusion **63**, 046010 (2023). https://doi.org/10.1088/1741-4326/acb785

18. J. Hillairet, V. Maquet, R. Ragona, T. Batal, S. Burles, Z. Chen, L. Colas, R. Dumont, F. Durand, F. Durodié, N. Faure, S. Garritta, L. Hijazi, I. Minondo, R. Mitteau, B. Salamon, B. Santraine, Overview of the WEST Ion Cyclotron Traveling Wave Array System Design, 25th Topical Conference on Radio-Frequency Power in Plasmas, Schloss Hohenkammer, Germany, May 19-22 (2025). https://www.ipp.mpg.de/5533880/